AIAA-2000-0907
Calculation of Wing flutter by a Coupled CFD-CSD method

F. Liu, J. Cai, Y. Zhu
University of California, Irvine
Irvine, CA 92697-3975

A.S.F. Wong, and H.M. Tsai
DSO National Laboratories
20 Science Park Drive, Singapore 118230

38th Aerospace Sciences Meeting & Exhibit
10-13 January 2000 / Reno, NV

Calculation of Wing Flutter by a Coupled CFD-CSD Method

F. Liu*, J. Cai†, Y. Zhu‡
Department of Mechanical and Aerospace Engineering
University of California, Irvine, CA 92697-3975

A.S.F. Wong§, H.M. Tsai¶
DSO National Laboratories
20 Science Park Drive, Singapore 118230

An integrated Computational Fluid Dynamics (CFD) and Computational Structural Dynamics (CSD) method is developed for the simulation and prediction of flutter. The CFD solver is based on an unsteady, parallel, multiblock, multigrid finite-volume algorithm for the Euler/Navier-Stokes equations. The CSD solver is based on the time integration of modal dynamic equations extracted from full finite-element analysis. A general multiblock deformation grid method is used to generate dynamically moving grids for the unsteady flow solver. The solutions of the flow field and the structural dynamics are coupled strongly in time by a fully implicit method. The unsteady solver with the moving grid algorithm can be used to calculate harmonic or indicial response of an aeroelastic system to be used by traditional flutter prediction methods on the frequency domain. The coupled CFD-CSD method simulates the aeroelastic system directly on the time domain and is not limited to linearized solutions. It is capable of predicting damped, diverging, and neutral motions, and limit cycle oscillations of an aero-elastic system. Computations are performed for a two-dimensional wing aeroelastic model and the the three-dimensional AGARD 445.6 wing. Flutter boundary predictions by the coupled CFD-CSD method are compared with those by the indicial method and experimental data for the AGARD 445.6 wing.

1 Introduction

Like in many other areas of aerodynamics, the panel method, methods based on the transonic small disturbance (TSD) equation, and methods based on the full potential (FP) equation successively found their ways in the simulation and prediction of flutter of airfoils and wings since CFD was introduced as a tool for aerodynamic research and design. As CFD and computer technology progress, higher order methods based on the Euler and the Navier-Stokes equations become more attractive since they are able to model more accurately transonic, nonlinear, and viscous effects. Computations have also advanced from two-dimensional problems to fully three-dimensional problems with or without coupled solution of the structural equations. Ballhaus and Goorjian[1] used a two-dimensional Euler code to calculate the indicial response of an airfoil, where the flow calculations were performed off-line, i.e., separately from the solution of the structural equations. Bendiksen and Kousen[2] and Kousen and Bendiksen[3] used an explicit time accurate Euler code to study nonlinear effects in transonic flutter. With their Euler model coupled with the solution of a 2 Degrees of Freedom (DOF) airfoil structural model, they demonstrated the possibility of Limit Cycle Oscillations (LCO) in a transonic flow. Lee-Rausch and Batina[4] and [5] developed three-dimensional methods for the Euler and Navier-Stokes equations, respectively, for predicting flutter boundaries of three-dimensional wings. Both the indicial method and the coupled CFD-CSD method was used. Guruswamy[6] developed a Navier-Stokes code, ENSAERO, for aeroelastic simulations.

It is clear that time accurate solutions with the coupled Euler/Navier-Stokes equations and the structural dynamic equations provide a powerful tool for simulating aerodynamic flutter phenomena. However, the computational time needed for such calculations still prevents such methods from being used for routine analysis and design purposes. In addition, the reliability and accuracy of such methods have not yet been well established.

An effective method to shorten the wall clock time for

*Associate Professor of Mechanical and Aerospace Engineering, senior Member AIAA.

†Visiting Research Specialist, Associate Professor, Northwestern Polytechnical University, Xi'an, China.

‡Graduate student, Member AIAA.

§Member of Technical Staff.

¶Senior Member of Technical Staff, Member AIAA.

such computations is to use parallel processing. Alonso and Jameson[7] developed a two-Dimensional parallel code for wing flutter calculations that couples the solution of the Euler equations with the solution of the structural equations. Byun and Guruswamy[8] also developed a parallel version of the ENSAERO code, which was recently used and extended by Goodwin, et al[9].

In this paper, we present a new integrated CFD-CSD simulation code for flutter calculations based on a parallel, multiblock, multigrid flow solver for the Euler/Navier-Stokes equations. Structural modal dynamic equations are solved simultaneously in a strongly coupled fashion with the Navier-Stokes equations by a fully implicit time marching method. A dual-time stepping algorithm is used to achieve time accuracy and allow simultaneous integration of the flow and structural equations without any time delay. A novel moving mesh method is developed to dynamically move/deform the computational grid at each time step. A spline matrix method is used to provide the interpolation between the CFD and CSD grids. The complete integrated CFD-CSD is implemented on a parallel computer by using the Message Passing Interface (MPI) standard. The code has been shown to offer good parallel speed-up on PC clusters networked with commodity 100Mb/s ethernet.

This computer program is capable of calculating conventional harmonic or indicial responses of an aeroelastic system as well as doing direct CFD-CSD simulations. Computations are performed on a two-dimensional airfoil model and a well established three-dimensional test case, the AGARD 445.6 wing[24, 25], to validate and establish the usefulness of the code. In the following section, we will describe each component of the integrated system. We will then present and analyze the computational results for the 2D aeroelastic wing model and the 3D AGARD 445.6 wing.

2 The Unsteady Navier-Stokes Solver

Tsai, Dong, and Lee[10] developed a multiblock, multigrid Euler/Navier-Stokes code called NSAERO (unfortunately, this is very close to the name of Guruswamy's code) for steady flow calculations based on Jameson's finite-volume and Runge-Kutta time-marching method[11, 12]. The multiblock algorithm uses two layers of halo cells to exchange flow information across a common interface between two blocks. Multigrid is implemented in a 'horizontal mode' as termed by Yadlin and Caughey[13], in which the block loop is nested inside the loop for the multigrid cycle so that information is exchanged among blocks and the flow field is updated on all blocks within each time step at each multigrid level. Information is not exchanged among blocks for the internal multi-stages of the explicit Runge-Kutta time-stepping within each time step. This code has been validated and extensively used for steady flow calculations of wing, wing-body combination, S-ducts, and complete aircraft[10].

In this research, the code is extended to perform time-accurate calculations. Time-accuracy is achieved by using the dual-time method proposed by Jameson[14]. The basic implementation of the dual-time step method is the same as in Liu and Ji[15]. After being discretized in space by a finite volume method, the time dependent Navier-Stokes equations can be written in the following semi-discrete form

$$\frac{dw}{dt} + R(w) = 0 \tag{1}$$

where w is the vector of flow variables at each mesh point, and R is the vector of the residuals, consisting of the spatially discretized flux balance of the Navier-Stokes equations. A second order accurate fully implicit scheme is then used to integrate the above equation in time,

$$\frac{3w^{n+1} - 4w^n + w^{n-1}}{2\Delta t} + R(w^{n+1}) = 0 \tag{2}$$

This implicit scheme is A-stable. We can reformulate (2) into the following

$$\frac{dw}{dt^*} + R^*(w) = 0 \tag{3}$$

where

$$R^*(w) = \frac{3}{2\Delta t}w + R(w) - \frac{2}{\Delta t}w^n + \frac{1}{2\Delta t}w^{n-1} \tag{4}$$

t^* is a pseudo-time. The solution of the implicit equation (2) is now made equivalent to the steady state solution of (3) with the pseudo-time t^*. We can then apply all the acceleration techniques including the multigrid method that are already implemented in the steady NSAERO to solving Equation (3). Once the solution to Equation (3) converges in pseudo-time, we achieve the time accurate solution to Equation (2) for one time step. As was demonstrated in [15], CFL numbers of more than 4000 could be used for solving the unsteady equations with this technique. Each time step needed about 20-40 multigrid pseudo-time cycles to reach a converged solution for the Euler equations. In the calculations performed in this paper, 60 pseudo-time cycles are used for each real time step when coupled with the structural modal equations to ensure adequate convergence in pseudo-time.

Time accurate calculations for three-dimensional problems are still very time consuming with even the

best algorithms available at the current time. In order to keep the computational time within realistic limits for large unsteady calculations, the code is also parallelized by using domain decomposition and MPI to take advantage of parallel computers or networked clusters of workstations. The flow field is partitioned into multiple blocks which are distributed over a number of processors available on a parallel computer or networked workstations. The existing multiblock structure in the steady NSAERO code[10] provides the basis for the parallel implementation. The dual time implicit-explicit solver is performed on each processor for the individual blocks assigned to that processor. Again, two layers of halo cells are used beyond the boundaries of each block to facilitate the implementation of boundary conditions and the communication between processors. Connectivity information of the blocks and processors are stored in preprocessed pointer arrays and MPI is used to perform the communication between blocks that are on different processors.

The unsteady implementation has been validated by calculating the same airfoil test case as in [15], i.e., the flow over a pitching NACA64A010 airfoil. Since the new unsteady parallel NSAERO code is fully three-dimensional, we also tested the airfoil case by laying the pitching airfoil in the three different coordinate planes. Comparison of the computed results showed no difference between the calculations with different coordinate orientations, and the results agree with the experimental data found in [16]. More detailed description of the parallel implementation and code validation studies will be presented in a separate paper.

In this paper, we will concentrate on flutter predictions to be discussed in the following sections. We will note, however, that the parallel code runs efficiently on clustered PCs. Figure 1 shows the parallel speedup for the airfoil case of the new parallel unsteady NSAERO running on the AENEAS computer consisting of 32 300MHZ Pentium II processors connected by a 100Mb switched ethernet network. It can be seen that the parallel efficiency remains high for the available processors for this case with 71001 total grid points. With 32 processors, we achieve a speedup factor of 25. The parallel efficiency is higher for most three-dimensional runs with more grid points.

3 A Multi-block Moving Mesh Algorithm

A novel moving grid algorithm, AIM3D, which remeshes the moving configuration adaptively in each block of grids, is also implemented in a parallel fashion and combined with the flow solver to handle flow problems with arbitrary motion of domain boundaries. The moving grid algorithm within each block is based on the method of arc-length based transfinite interpolation which is performed independently on local processors where the blocks reside. A spring network approach is used to determine the motion of the corner points of the blocks which may be connected in an unstructured fashion in a general multi-block method. A smoothing operator is applied to the points of the block face boundaries and edges in order to maintain grid smoothness and grid angles. The details of this moving grid method is described in [17]

4 The CSD Model and Its Solution

Modal equations are used to calculate the structural deformation under an aerodynamic forcing. For each mode i, the modal dynamic equation is written in the following form

$$\ddot{q}_i + 2\zeta_i\omega_i\dot{q}_i + \omega_i^2 q_i = Q_i \tag{5}$$

where q_i is the generalized normal mode displacement, ζ_i is the modal damping, ω_i is the modal frequency, and Q_i is the generalized aerodynamic force. The structural displacement vector can be written as a summation of N modal shapes extracted from a full finite element analysis of the structure.

$$\{u_s\} = \sum_{i=1}^{N} q_i\{h_i\} \tag{6}$$

where $\{h_i\}$ are the modal shapes.

Equation (5) is converted into a first order system of equations for each i and integrated in time by a second-order fully implicit scheme. Following Alonso and Jameson[7], we assume

$$\begin{aligned} x_{1i} &= q_i \\ \dot{x}_{1i} &= x_{2i} \\ \dot{x}_{2i} &= Q_i - 2\zeta_i\omega_i x_{2i} - \omega_i^2 x_{1i} \end{aligned} \tag{7}$$

for each of the modal equations. We can rewrite the above equations in matrix form as

$$\{\dot{X}_i\} = [A_i]X_i + \{F_i\}, \quad i = 1, N \tag{8}$$

where $\{X_i\} = \left\{ \begin{array}{c} x_{1i} \\ x_{2i} \end{array} \right\}$, $[A] = \left[\begin{array}{cc} 0 & 1 \\ -\omega_i^2 & -2\omega_i\zeta_i \end{array} \right]$ and $\{F_i\} = \left\{ \begin{array}{c} 0 \\ Q_i \end{array} \right\}$. After proper diagonalization, the above equation can be decoupled.

$$\frac{dz_{1i}}{dt} = \omega_i(-\zeta_i + \sqrt{\zeta_i^2 - 1})z_{1i} + \frac{(-\zeta_i + \sqrt{\zeta_i^2 - 1})}{2\sqrt{\zeta_i^2 - 1}}Q_i \tag{9}$$

$$\frac{dz_{2i}}{dt} = \omega_i(-\zeta_i - \sqrt{\zeta_i^2-1})z_{2i} + \frac{(\zeta_i + \sqrt{\zeta_i^2-1})}{2\sqrt{\zeta_i^2-1}}Q_i \quad (10)$$

We use the same second order accurate fully implicit scheme as Equation (2) to integrate the above equations in time.

$$\frac{3z_{1i}^{n+1} - 4z_{1i}^{n} + z_{1i}^{n-1}}{2\Delta t} = -R_{1i}(z_{1i}^{n+1}, z_{2i}^{n+1}, Q_i^{n+1}) =$$
$$\omega_i(-\zeta_i + \sqrt{\zeta_i^2-1})z_{1i}^{n+1} + \frac{(-\zeta_i + \sqrt{\zeta_i^2-1})}{2\sqrt{\zeta_i^2-1}}Q_i^{n+1} \quad (11)$$

$$\frac{3z_{2i}^{n+1} - 4z_{2i}^{n} + z_{2i}^{n-1}}{2\Delta t} = -R_{2i}(z_{1i}^{n+1}, z_{2i}^{n+1}, Q_i^{n+1}) =$$
$$\omega_i(-\zeta_i - \sqrt{\zeta_i^2-1})z_{2i}^{n+1} + \frac{(\zeta_i + \sqrt{\zeta_i^2-1})}{2\sqrt{\zeta_i^2-1}}Q_i^{n+1} \quad (12)$$

The variables z_{1i}, z_{2i}, and Q_i in the above equations are coupled through the flow equations. The deformation of the wing, i.e., z_{1i}, z_{2i} influences the flow field and, thus, the aerodynamic force Q_i. Conversely, the aerodynamic force Q_i determines the deformation of the wing. Therefore, the above equations for the time marching of the structural equations must be solved simultaneously with Equation (2) for the Navier-Stokes equations.

It is very convenient to reformulate Equations (11) and (12) into an identical pseudo-time format as Equations (3) and (4), i.e.,

$$\frac{dz_{1i}}{dt^*} + R_{1i}^*(z_{1i}, Q_i) = 0 \quad (13)$$

$$\frac{dz_{2i}}{dt^*} + R_{2i}^*(z_{2i}, Q_i) = 0 \quad (14)$$

where

$$R_{1i}^*(z_{1i}, Q_i) = \frac{3}{2\Delta t}z_{1i} + R_{1i}(z_{1i}, z_{2i}, Q_i) - \frac{2}{\Delta t}z_{1i}^{n} + \frac{1}{2\Delta t}z_{1i}^{n-1} \quad (15)$$

$$R_{2i}^*(z_{1i}, Q_i) = \frac{3}{2\Delta t}z_{2i} + R_{2i}(z_{1i}, z_{2i}, Q_i) - \frac{2}{\Delta t}z_{2i}^{n} + \frac{1}{2\Delta t}z_{2i}^{n-1} \quad (16)$$

Equations (3), (13) and (14) can be regarded as one single system of time dependent equations in the pseudo-time t^* which can be solved by existing efficient explicit time marching methods until a steady state is reached. Once the computation reaches a steady state in the pseudo-time t^*, the solutions to Equations (3), (13) and (14) then become the time accurate solution of the implicit fully coupled CFD-CSD Equations (2), (11) and (12) in one physical time step without any time lag between the CFD and CSD equations.

In the current implementation, the same 5 stage Runge-Kutta time stepping scheme for the Navier-Stokes equations is used for the CSD equations. It is found, however, that the CSD pseudo-time equations converge faster than their counterparts in the flow equations. Therefore, it is more efficient and, in fact, more robust to march the flow equations with more pseudo-time steps than for the CSD equations. It should be noticed that this will not affect the final time accuracy in the physical time as long as a steady state is reached in the pseudo-time.

5 Interfacing between the CSD and CFD Grids

The proceeding sections lay out the mathematical formulation of the coupling of the CFD and CSD equations. However, there remains a missing link in actual computation, that is, the relation between the CFD computational grid and the CSD computational grid. Although Bendiksen and Hwang[21] developed a finite element algorithm for both the flow equations and the structural equations so that the same surface grid can be used, most CFD codes use different algorithms and different computational grids for the flow and the structures. Consequently, interpolation of computational grids and aerodynamic loads must be performed between the two systems. A suitable method that handles this need in a general fashion is still in the making. The current engineering practice, as exemplified in MSC/NASTRAN and used in the current paper, uses a combination of methods. The infinite plate spline (IPS) by Harder and Desmarais[18] and thin plate spline (TPS) by Duchon[19] is more suitable for wing-like components where the structure is usually modeled by plate and shell elements. The beam spline method by Done[20] is used for body-like component as the structure is modeled by beam elements. The structural grid of a complex structure that uses a combination of different elements can be related to the aerodynamic grid by using different spline methods. Details of the approach are to be found in MSC/NASTRAN Aeroelastic Analysis, User's Guide. Once a spline method is applied, the displacement vector defined on the structural grid $\{u_s\}$ can be related to the displacement vector on the aerodynamic grid $\{u_a\}$ via a spline matrix $[G]$,

$$\{u_a\} = [G]\{u_s\} \quad (17)$$

Once the structure equations are solved, the displacements on the structural grid $\{u_s\}$ is transformed to the displacement on the aerodynamic grid $\{u_a\}$ by the above equation, from which the deforming grid code AIM3D discussed in Section 3 can then be used to regenerate the volume grid in the flow field for CFD computations. Once the flow equations are solved, the

aerodynamic loading on the CFD grid $\{F_a\}$ can then be transformed to the aerodynamic loading on the structural grid $\{F_s\}$ via the following equation based on the principle of virtual work.

$$\{F_s\} = [G]^T \{u_a\} \tag{18}$$

where $[G]^T$ is the transpose of $[G]$. Equation (18) guarantees the conservation of energy between the flow and the structural systems due to the fact that it is derived by the principle of virtual work.

The size of the vector $\{u_a\}$ is 3 times m, m being the number of aerodynamic grid points on the wing surface. The size of the structural displacement vector $\{u_s\}$ is 3 times n, n being the number of finite element grid point on the wing surface. The size of the $[G]$ matrix is then $(3m) \times (3n)$. The $[G]$ matrix is pre-generated and stored in the code.

6 The Integrated Aero-structure System

Figure 2 shows the integration strategy for our aeroelastic simulation system. At the start of the program, specification of the structures are input to NASTRAN which extracts the modal shapes and parameters needed by the CSD solver in the coupled simulation code. Inputs are also given to the flow solver NSAERO and its preprocessor PREPNS. The flow solver will first compute the static loading on the structure. The aerodynamic forcing $\{F_a\}$ is then transformed to the form suitable for the CSD modal equations using the SPLINE matrix G. The CSD solver then computes the structural displacement $\{u_s\}$, which is subsequently transformed to the grid points for the flow solver. With the new displacement $\{u_a\}$, the dynamic moving mesh program REMESH (AIM3D) is called to regenerate the mesh for the flow solver. The flow solver and the CSD solver are coupled within each time step through the above process as shown by the arrows in Figure 2. Since both the flow equations and the structural equations are solved by a pseudo-time iteration algorithm, the above coupling between the CFD and CSD solver are easily absorbed in the pseudo-time iteration process until a fully converged solution is achieved at the new time level as discussed in Section 4.

Figure 2 also shows a "decoupled" approach for flutter prediction marked by the dashed lines. In such an approach, prescribed structural motion is provided to the flow solver without being coupled with the CSD model. The generalize aerodynamic force Q_{ij} on the frequency domain is extracted from the CFD calculations by using either the harmonic method or the indicial response method. Q_{ij} will then be fed into the conventional V-g method to obtain flutter boundaries of the aero-elastic system. This method provides a fast tool for flutter predictions, but it is restricted to linear systems. The fully coupled method provides a compliment to the linearized approach.

7 Computational Results

7.1 A two-Dimensional Wing Model

As a first test case, we apply the coupled CFD-CSD method to the two-dimensional Isogai wing model[22, 23], Case A. This model simulates the bending and torsional motion of a wing cross-section in the outboard portion of a swept wing. It consists of two degrees of freedom, plunging and pitching, for a NACA 64A010 airfoil. We compute this case with the Euler equations and compare the results by Alonso and Jameson[7]. The details of the structural model can be found in [7] as well as in [22] and [23].

Figures 3-6 show the flutter computational results for the Isogai wing model at a flight Mach number of 0.825. Plotted in the figures are the time history of the pitching and plunging amplitude computed by the integrated CFD-CSD code with the fully coupled CFD and CSD approach. Figure 3 is a case with a low speed index $V_f = 0.530$. V_f is defined as

$$V_f = \frac{U_\infty}{b\omega\sqrt{\mu}}$$

where U_∞ is the freestream velocity, b is the half chord, ω is the structural frequency, μ is the mass ratio. For this low V_f, figure 3 shows that both the pitching and plunging amplitude decays with time, indicating that the aeroelastic system is stable for this particular condition. At a higher V_f, the system may become less and less stable until one or both of the pitching and plunging motions diverge as shown in Figure 4 when $V_f = 0.725$. In between these two V_f conditions, there is a particular point where the system is neutrally stable. This is shown in Figure 5 when $V_f = 0.630$.

A converging point and a diverging point like the above are first identified, from which we can interpolate the V_f in between to obtain an estimate of the neutral point. We then perform a computation with the new V_f to see if it is above or below the stability limit, or perhaps right at the neutral point. It may take several runs for a given freestream Mach number before the V_f corresponding to the neutral stability point can be accurately located by this 'bi-section' method. However, most of the runs do not need computations with many time periods since we can easily identify whether the system is oscillating with a diverging or converging amplitude by looking at only the first few periods.

With this method computations for a number of freestream Mach numbers for the Isogai wing model are performed. The flutter boundary predicted by our code is plotted and compared with that obtained by Alonso and Jameson[7] in Figure 7. Clearly, the results by the two codes agree very closely for this case.

Figure 6 shows a situation where the system initially diverges but then reaches a steady oscillatory mode with finite amplitude, the so-called Limit Cycle Oscillation (LCO). The LCO for this case was first discovered by Kousen and Bendiksen and was also shown by Alonso and Jameson[7]. This test case demonstrates the capability of the integrated CFD-CSD program to predict LCO although the computation may have to be performed for a long time before LCO can be identified in the time integration.

7.2 The AGARD 445.6 Wing

Although the results in the above section are calculated by using the full three-dimensional code with 8 cells in the spanwise direction, the flow is only two-dimensional. In this section, the integrated aeroelastic system is used to predict the flutter boundary for the AGARD 445.6 wing[25, 24] by both the indicial method and the coupled CFD-CSD method. This wing is a semispan model made of the NACA 65A004 airfoil that has a quarter-chord sweep angle of 45 degrees, a panel aspect ratio of 1.65, and a taper ratio of 0.66. We consider the weakened wing model as listed in Reference [24]. It was tested in the Transonic Dynamics Tunnel (TDT) at NASA Langley Research Center. This is a well-defined test case proposed as an AGARD standard aeroelastic configuration for flutter calculations[25]. The wing is modeled structurally by the first four natural vibrational modes shown in Figure 8 as taken from Reference [25]. Those are identified as the first bending, first torsion, second bending, and second torsion modes, respectively, by a finite-element analysis. The natural frequencies of these modes are also shown in Figure 8. A grid of 176601 is used for this case. Although the code is capable to run in the Navier-Stokes mode with a two-equation k-ω model, only Euler solutions are presented in this work.

In a harmonic method to calculate the generalize aerodynamic force Q_{ij} for the i-th vibrational mode, the wing is assumed to undergo a sinusoidal motion of the i-th mode at a given reduced frequency κ. The unsteady flow induced by this sinusoidal motion is then calculated, from which the generalized aerodynamic force on each of the j-th mode ($j = 1, 4$) can be deduced. To illustrate the shape and motion of the wing, Figure 9 shows the computed pressure distribution in the symmetry plane and on the wing surface at one time instant for the four different wing structural deformation modes vibrating sinusoidally at their corresponding natural frequencies, respectively.

In order to use a classical V-g method to determine the flutter boundary, Q_{ij} must be calculated over a range of frequencies of interest. Consequently, computation of the flow field must be performed for a number of reduced frequencies and for each vibrational mode of importance in a harmonic method. This demands a large amount of computational time. An alternative is to use the Indicial Method originally proposed by Tobak[26], and also by Ballhaus and Goorjian[1], in which, a step function input excitation is fed into the aerodynamic system for each structural mode. The response of the aerodynamics system is called the Indicial Response. A Fourier analysis on this Indicial Response is enough to deduce the system response $Q(\kappa)$ for the complete range of the reduced frequency κ. In this way, only one time-integration of the Euler/Navier-Stokes equations is needed for each mode of the structural system in order to obtain the complete GAF matrix $Q_{ij}(\kappa)$. Seidel, Bennett and Ricketts[27] introduced a impulse function method to avoid the discontinous nature of the step function used by Ballhaus and Goorjian[1]. The impulse method is used in this work.

Figures 10 and 11 show the comparison of the generalized aerodynamic forces Q_{11} and Q_{21} calculated by the harmonic method and the impulse method for the 445.6 wing at a freestream Mach number $M_\infty = 0.901$. It can be seen that except near the high reduced frequency end, the indicial method based on the impulse input agree well with the harmonic method. The indicial method, however, significantly reduces the computational time.

Figures 12, 13, 14, and 15 show the computed generalized aerodynamic forces Q_{11}, Q_{12}, Q_{21}, and Q_{22}, respectively, by the indicial method for the first two vibrational modes. The first 4 modes are calculated although only 2 of them are shown here. Those Q_{ij}'s are then used in a classical V-g method code to determine the flutter boundary of the wing.

Unlike in an indicial or harmonic method where a prescribed motion of the wing is used, the motion of the wing is not pre-determined in a direct CFD-CSD coupled simulation. It is computed based entirely on the flow and structural dynamic equations and their interaction. The wing is started with either an initial displacement and zero initial vibrational velocity or zero displacement but non-zero vibrational velocity in each of the 4 modes. A steady state solution is first obtained for a given initial position of the wing and then the wing is let go. The wing will then start oscilating in time resulting in either damped, diverging,

or neutral vibrations.

Figures 16 to 19 show the time histories of the generalize coordinates q_i of the first 4 modes in the coupled CFD-CSD unsteady computations for some different flight Mach numbers and different speed index V_f. Although the time history may be different when different initial conditions are used, it was found that the general behavior of the wing is the same in so far as stability is concerned. If a mode is unstable (diverging in time) for the zero velocity but non-zero displacement initial condition, it will also be unstable for the zero displacement but non-zero velocity initial condition. In principle, it is not impossible that stability depends on initial conditions for a nonlinear system. However, no special effort is made to identify this in the current work.

Consider the supersonic flight condition $M_\infty = 1.141$ tested in the experiment[24]. Figure 16 shows the time history of the 4 generalized coordinates for the 445.6 wing for a velocity index $V_f = 0.58$. For this case, the flow is started with zero initial displacement but a non-zero initial velocity in all of the four modes of the wing. Clearly, Figure 16 shows that this is a damped case. The amplitudes of all modes decrease in time. Therefore, the system is stable for this condition. At a little higher speed index $V_f = 0.652$, the system exhibit high vibrational amplitude and slower damping as shown in Figure 17. However, it is still a damped case although it is getting close to the neutral condition. At an even higher speed index $V_f = 0.70$ as shown in Figure 18, we can see that the amplitude of the first three modes grow very fast, indicating that we have passed the neutral stability point. At this point, the flutter boundary for this flight Mach number can be roughly estimated to be in between $V_f = 0.652$ and $V_f = 0.700$. This process can be iterated to obtain better estimates of the flutter boundary. But for this case, a mean value from $V_f = 0.652$ and $V_f = 0.700$ will suffice considering the large difference between the experimental data and the computed data to be discussed later.

The flutter mode can be determined by looking at these figures and identify which mode first starts to be unstable as we increase the V_f. Once this mode is identified, a Fourier analysis of this mode can be performed in its last few periods of vibration near the neutral point to identify its frequency. A quick estimate can be obtained by simply measuring the time between the two zero points in the end of the vibration. This may get somewhat ambiguous in some cases in determining the flutter mode and flutter frequency. It is noticed, however, from Figures 16-18 that the vibrational frequencies of the 4 modes initially are rather different and closer to their natural frequencies for the low V_f case. As the speed index increases, the low frequency modes shift to higher frequencies, while the high modes tend to shift towards the low frequency end. Near the neutral point, the first two modes tend to oscillate at the same frequency.

Figure 19 shows the calculation for the condition $M_\infty = 1.072$ and $V_f = 0.46$. Clearly, this shows that the V_f is at or very close to the flutter boundary and that the first or the second mode is the flutter mode, which are almost neutral and oscillate at almost equal frequency while the higher modes damp out in time.

Figure 20 shows a similar calculation for the subsonic condition $M_\infty = 0.901$ and $V_f = 0.34$. Again, this shows that the chosen V_f is at or very close to the flutter boundary and that the first mode is the flutter mode since all other modes are being damped. It is noticed that the frequency of the higher modes remain high in this case.

Using the above approach, we determined the flutter boundary and frequency of the weakened wing over the flight Mach number range $M_\infty = 0.338$ to 1.141 studied experimentally in [24]. The results are shown in Figures 21 and 22 together with the experimental data and those calculated by the V-g methods based on the calculated indicial responses. It can be seen that the results computed by the coupled CFD-CSD method agree very well with the experimental data in the subsonic and transonic range.

In the supersonic range, however, both the coupled method and the indicial method yield much higher flutter velocities than those determined in the experiment. It is also to be noticed that Reference [4] also overpredicted the V_f for supersonic flight conditions by almost equal amount compared to our result. Although [5] and [9] showed some improvement by performing full Navier-Stokes calculations, the amount of improvement was small compared to the still large differences between their computational results and the experiment. It is not clear why this is the case. However, subtle differences between the subsonic and supersonic cases can be observed from the time histories shown in Figures 16 to 20. In the subsonic case shown in Figure 20, the damped modes show monotonically decreasing amplitudes similar to those found for the two-dimensional airfoil case shown in Figure 3. For the supersonic cases, however, the first mode shows a clear growth before it starts to decay (Figures 16 and 17) or being neutral (Figure 19). This behavior is found to be independent of the initial conditions used in the calculations. It might be conjectured that this nonlinear behavior can be responsible for the early detection of flutter in the model wing tested in [24]. Further investigation is necessary in this regard.

It has been suggested that LCO may be indicated in the V-g analysis if it exists. The coupled CFD-CSD approach may then be used to confirm the existence of LCO. However, no LCO phenomenon for the 445.6 wing has been found in this research or by any other researchers.

8 Concluding Remarks

A parallel integrated CFD-CSD simulation program has been developed for the simulation and prediction of flutter of an aeroelastic system. This program consists of a three-dimensional, parallel, multi-block, multigrid, unsteady Navier-Stokes solver, a parallel dynamic grid deformation code, a CSD solver strongly coupled with the flow solver using dual time stepping, and a spline matrix method for interfacing the CFD and CSD grid and aerodynamic loading variables. This program has two options. Option 1 allows it to obtain the harmonic or indicial responses of an aeroelastic system by prescribing the motion of the structure. Option 2 uses the coupled CFD-CSD method to directly simulate the unsteady behavior of an aeroelastic system. Flutter speed, mode, and frequency can be determined by analyzing the time history of the structural vibration.

The code has been used to simulate transonic flutter of a 2D airfoil, and the three-dimensional AGARD 445.6 wing by both the indical method option using an impulse input and the coupled CFD-CSD option. Some useful observations are summarized below:

- In the indical method approach, as many runs as there are structural modes must be performed to determine the generalized aerodynamic forces needed by the V-g method to determine flutter boundary. Typically for a wing, 4 modes are needed. Each run must be performed with adequate time resolution in order to accurately calculate the aerodynamic response for high frequencies. In addition, long time periods are also needed for the disturbances due to the initial impulse to sufficiently decay.

- The coupled CFD-CSD option consists of a series of full simulations of an aeroelastic system with some arbitrarily chosen initial perturbation of the aero-structure system, much like in wind tunnel test. Flutter is detected by examining the computed structural displacements to see if the initial perturbations will decay, grow, or maintain a neutral stance. This is readily noted within 2 to 3 periods of oscillations for most situations, which may actually be less time than one run in the indicial method mode. To determine the neutral point, 3 or more runs are usually needed.

- The stability quality determined by the above approach does not depend on the choice of initial conditions for the computations done in this paper.

- Signal analysis of the calculated modal displacements in the direct coupled method must be performed in order to determine the flutter mode, speed, and frequency. Ambiguity may exist in this method in determining which mode is the flutter mode and at what frequency. For the AGARD 445.6 wing case, however, it was found that flutter appears to happen with mostly the first and second modes. The frequencies of these two modes tend to approach each other as the velocity index approaches the neutral point.

- Both methods give almost identical results of the flutter speed and flutter frequency for the AGARD 445.6 wing. If one has a rough idea of where flutter might occur, the coupled CFD-CSD method can give us an estimate of the flutter point more quickly than the indicial method.

- Flutter speed and flutter frequency predictions by the coupled approach agree very well with experimental data for subsonic and transonic speeds. The transonic dip phenomena is well captured.

- For subsonic cases, the coupled approach predicts either monotonically decaying modes or monotonically growing modes for velocity index values below or above the numerically determined neutral point.

- Both the indicial method and the coupled method over-predict the flutter speed and flutter frequency for the AGARD 445.6 wing at supersonic speeds. The coupled approach, however, predicts consistent initial growths of the structural motions before they decay for velocity index values above the experimental data but below the numerically determined neutral points. Monotonic growth is observed when the velocity index is above the numerically determined neutral point. Whether this offers an explanation for the discrepancy between the experimental data and the numerical computation for the supersonic case needs further investigation.

- The coupled CFD-CSD option may be used to simulate and predict LCO. However, long time of computation may be needed in order to see if a system will enter into an LCO mode. Other quick methods may be used to indicate the possibility of LCO.

The coupled approach may then be used to confirm and simulate the LCO motion.

- The program developed scales well on networked PC clusters with commodity 100Mb/s ethernet connections. Parallel efficiencies of 25 is reached on 32 networked Pentium II 300Mhz PCs for small two-dimensional problems. Higher parallel efficiencies can be achieved for larger grid sizes. Work is in progress to test it on larger parallel systems in addition to networked PCs.

- With 32 networked Pentium II 300 MHz PCs, one run of 3 periods in the coupled mode takes about 12 hours for the AGARD 445.6 wing with 176,601 grid points and 64 time steps per period. With the fast advance in computer hardware, further improvement in the computational algorithms, and better optimization of the computer program, the CFD-CSD coupled approach may be not so far off from being used for routine applications.

9 Acknowledgement

Computations of this work has been performed on the AENEAS parallel computer system in UC Irvine.

References

[1] Ballhaus, W.F. and Goorjian, P.M., "Computation of Unsteady Transonic Flows by the Indical Method," AIAA Journal, Vol. 16, No. 2, Feb. 1978, pp.117-124.

[2] Bendiksen, O. O., and Kousen, K. A., "Transonic Flutter Analysis Using the Euler Equation,", AIAA Paper 87-0911, April, 1987.

[3] Kousen, K. A., and Bendiksen, O. O., "Limit Cycle Phenomena in Computational Transonic Aeroelasticity," Journal of Aircraft, Vol. 31, No. 6, pp. 1257-1263, November-December, 1994.

[4] Lee-Rausch, E. M., Batina, J. T., "Wing Flutter Boundary Prediction Using Unsteady Euler Aerodynamic Method", Journal of Aircraft, Vol. 32, No. 2, pp. 416-422, March-April, 1995.

[5] Lee-Rausch, E. M., Batina, J. T., "Wing Flutter Computations Using an Aerodynamic Model Based on the Navier-Stokes Equations", Journal of Aircraft, Vol. 33, No. 6, pp. 1139-1147, November-December, 1996.

[6] Guruswamy, G. P., "Navier-Stokes Computations on Swept-Tapered Wings, Including Flexibility," AIAA Paper 90-1152, April, 1990.

[7] Alonso J. J., and Jameson, A. , "Fully-Implicit Time-Marching Aeroelastic Solutions", AIAA Paper 94-0056, Jan., 1994.

[8] Byun, C., Guruswamy, G. P., "Aeroelastic Computations on Wing-Body-Control Configurations on Parallel Computers," AIAA Paper 96-1389, April, 1996.

[9] Goodwin, S.A., Weed, R. A., Sankar, L. N., and Raj, P., "Toward Cost-Effective Aeroelastic Analysis on Advanced Parallel Computing Systems," Journal of Aircraft, Vol. 36, No. 4, pp. 710-715, July-August, 1999

[10] Tsai, H. M., Dong, B., and Lee, K. M., "The Development and Validation of a Three-dimensional Multiblock, Multigrid Flow Solver for External and Internal Flows," AIAA Paper 96-0171, January, 1996.

[11] Jameson, A., Schmidt, W., and Turkel, E., "Numerical Solutions of the Euler Equations by Finite Volume Methods Using Runge-Kutta Time-Stepping Schemes," AIAA Paper 81-1259, June 1985.

[12] Jameson, A., "Multigrid Algorithms for Compressible Flow Calculations," MAE Report 1743, Princeton Univ., NJ, text of lecture given at 2nd European Conference on Multigrid Methods, Cologne, FRG, Oct. 1985.

[13] Yadlin, Y., and Caughey, D.A., "Block Multigrid Implicit Solution of the Euler Equations of Compressible Fluid Flow," AIAA-90-0106, January 1990

[14] Jameson, A., "Time Dependent Calculations Using Multigrid, with Applications to Unsteady Flows past Airfoils and Wings," AIAA Paper 91-1596, 10th AIAA Computational Fluid Dynamics Conference", June, 1991.

[15] Liu, F. and Ji, S., "Unsteady Flow Calculations with a Multigrid Navier-Stokes Method," AIAA Journal, Vol. 34, No. 10, 1996, pp. 2047-2053.

[16] Davis, S. S., "NACA64A010 Oscillatory Pitching," in Compendium of Unsteady Aerodynamics Measurements, AGARD-R-702, 1982.

[17] Wong, A. Tsai H., Cai, J., Y. Zhu, and F. Liu, "Unsteady Flow Calculations with a Multi-Block Moving Mesh Algorithm", AIAA Paper 2000-1002, Jan., 2000.

[18] Harder, R. L., Desmarais, R. N., "Interpolation Using Surface Splines", Journal of Aircraft, Vol. 9, No. 2, February 1972, pp. 189-191.

[19] Duchon, J. P., "Splines Minimizing Rotation-Invariant Semi-Norms in Sobolev Spaces, in Schempp, W. and Zeller, K, editors, Constructive Theory of Functions of Several Variables, Oberwolfach 1976, pp. 85-100, Springer-Verlag, Berlin, 1977.

[20] Done, G. T. s., "Interpolation of Mode Shapes: A Matrix Scheme Using Two-Way Spline Curves", Aeronautical Quarterly, Vol. 16, November 1965, pp.333-349.

[21] Bendiksen, O. O., and Hwang, G., "Nonlinear Flutter Calculations for Transonic Wings," Proc. Int. Forum on Aeroelasticity and Structure Dynamics, June 17-20, 1997, pp105-114, Rome, Italy.

[22] Isogai, K., "On the Transonic-Dip Mechanism of flutter of a Sweptback Wing," *AIAA Journal*, Vol. 17, No. 7, pp.793-795, 1979.

[23] Isogai, K., "On the Transonic-Dip Mechanism of flutter of a Sweptback Wing: Part II," *AIAA Journal*, Vol. 19, No. 7, pp.1240-1242, 1981.

[24] Yates, E.C, Jr., Land, N.S. and Foughner J.T. Jr, "Measured and Calculated Subsonic and Transonic Flutter Characteristics of a 45° Swepteback Wing Planform in Air and in Freon-12 in the Langley Transonic Dynamics Tunnel", NASA TN D-1616, March, 1963.

[25] AGARD Standard Aeroelastic Configurations for Dynamic Response I – Wing 445.6, NASA TM 100492, Aug., 1987.

[26] Tobak, M., "On the Use of Indicial Function Concept in the Analysis of Unsteady Motions of Wings and Wing-Tail Combinations," NACA Report, 1188, 1954.

[27] Seidel, D.A., and Bennet, R.M., "An Exploratory Study of Finite-Difference Grids for Transonic Unsteady Aerodynamics," AIAA 83-0503, Jan. 1983.

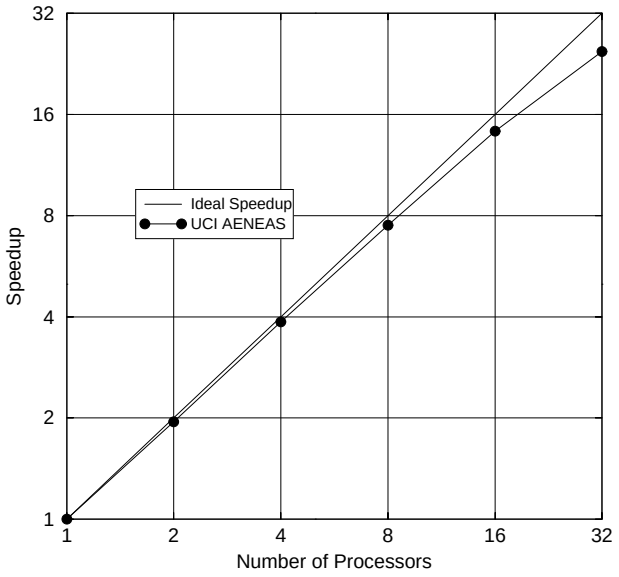

Figure 1: Parallel Speedup for the Parallel Unsteady NSAERO Code on a 32 node PC Cluster with 100Mb Switched Ethernet, 71001 grid points

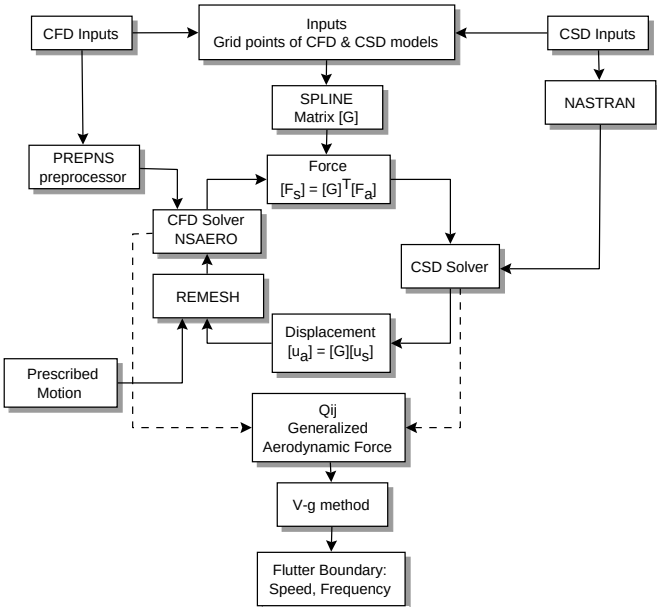

Figure 2: Integrated CFD-CSD Method for Flutter Calculations

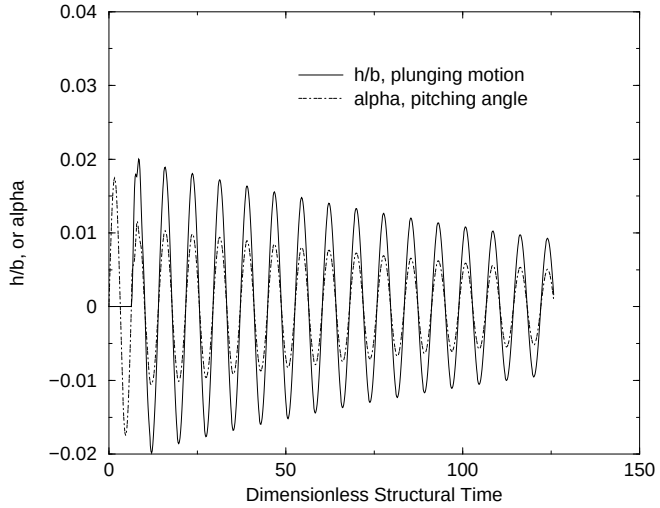

Figure 3: Time history of pitching and plunging motion for the Isogai wing model for $M_\infty = 0.825$, and $V_f = 0.530$

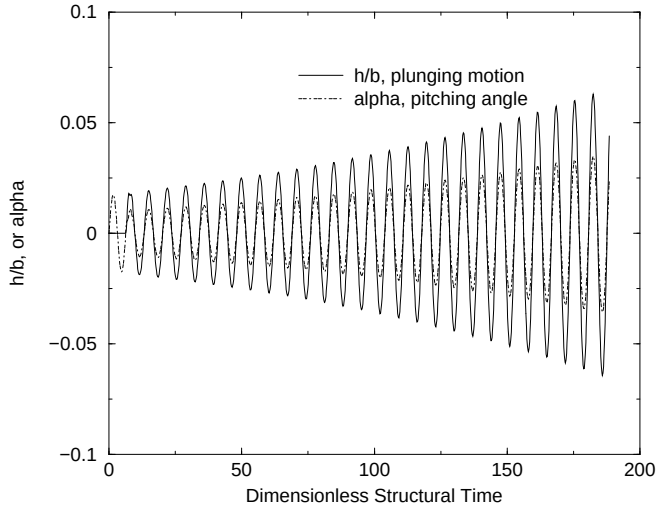

Figure 4: Time history of pitching and plunging motion for the Isogai wing model for $M_\infty = 0.825$, and $V_f = 0.725$

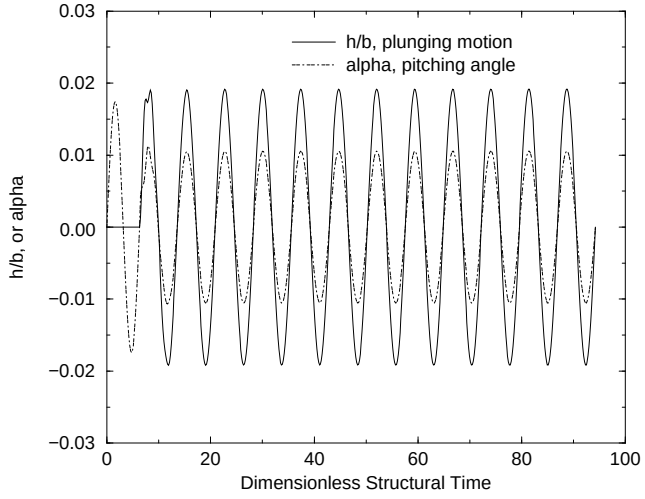

Figure 5: Time history of pitching and plunging motion for the Isogai wing model for $M_\infty = 0.825$, and $V_f = 0.630$

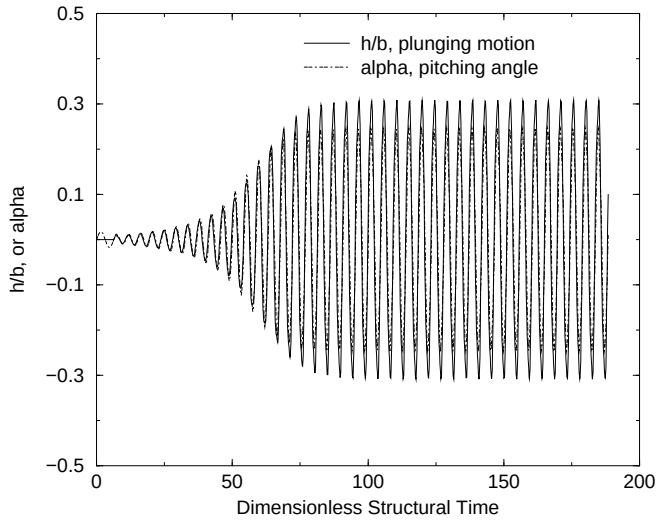

Figure 6: Time history of pitching and plunging motion for the Isogai wing model for $M_\infty = 0.75$, and $V_f = 1.33$

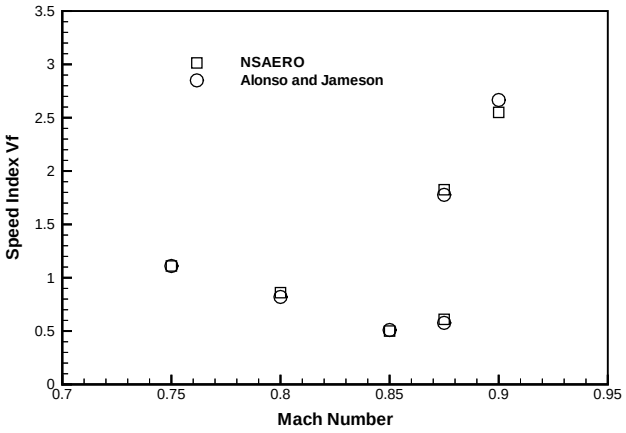

Figure 7: Flutter Boundary Predicted by NSAERO Compared to that by Alonso and Jameson[7]

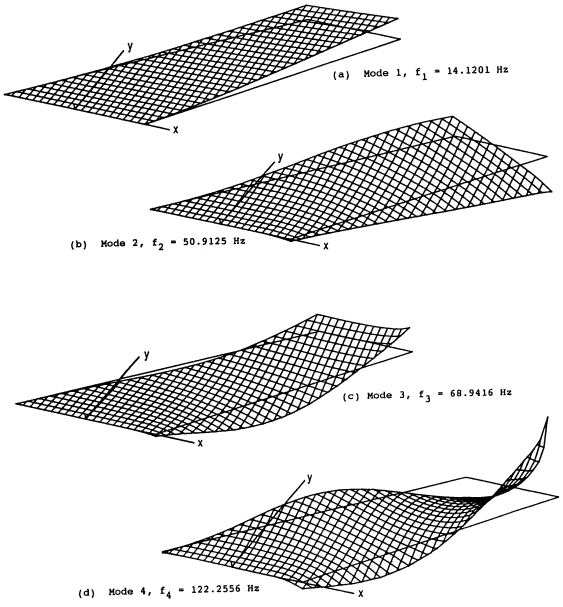

Figure 8: Modal deflections for the 445.6 Wing

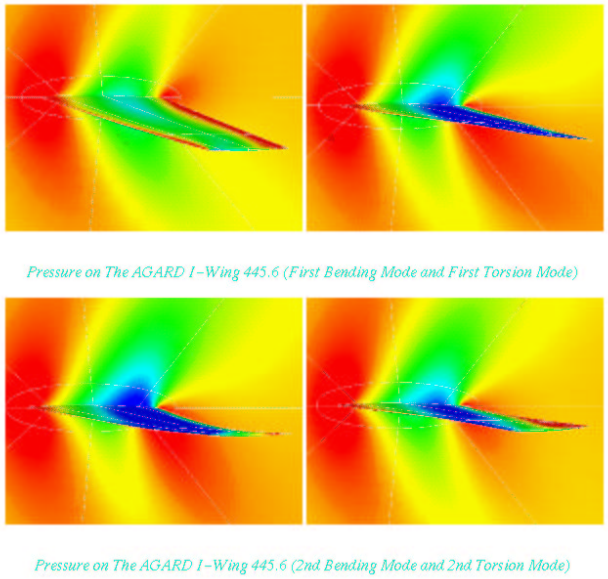

Figure 9: Pressure distributions in the symmetry plane and on the 445.6 wing surfaces at one instant during oscillation of each of the 4 vibrational modes

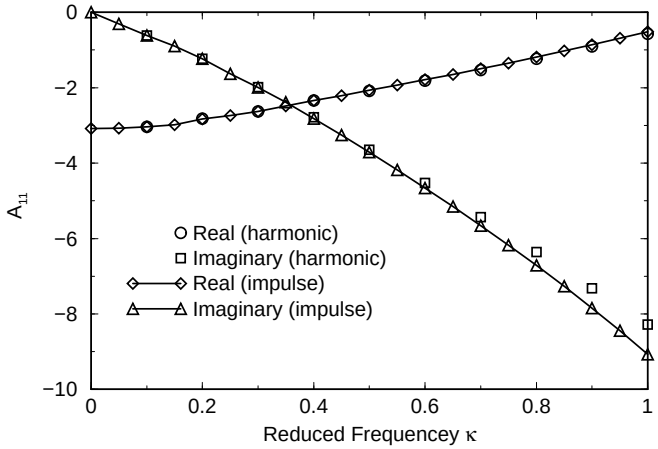

Figure 10: Comparison of generalized aerodynamic forces calculated by the harmonic and indicial methods Q_{11} for $M_\infty = 0.901$

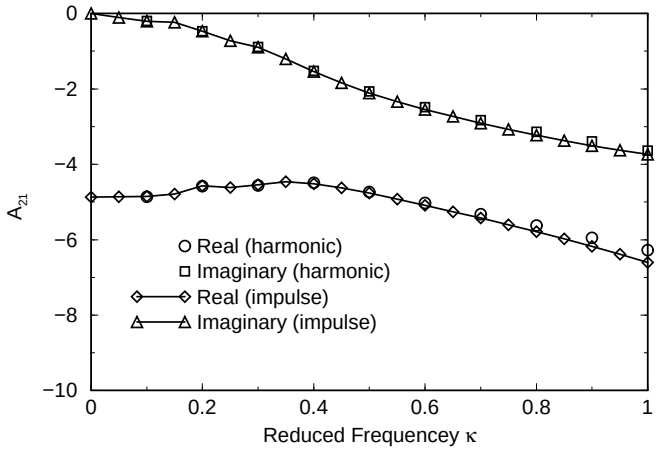

Figure 11: Comparison of generalized aerodynamic forces calculated by the harmonic and indicial methods Q_{21} for $M_\infty = 0.901$

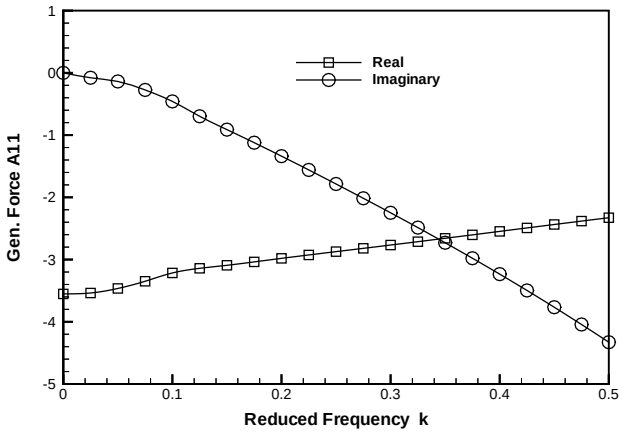

Figure 12: Generalized aerodynamic force Q_{11} for $M_\infty = 0.960$

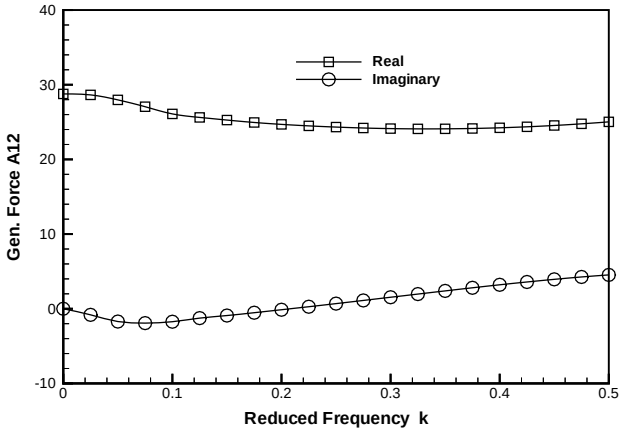

Figure 13: Generalized aerodynamic force Q_{12} for $M_\infty = 0.960$

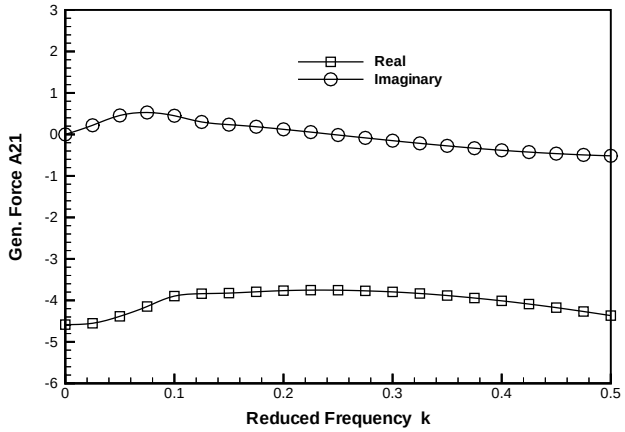

Figure 14: Generalized aerodynamic force Q_{21} for $M_\infty = 0.960$

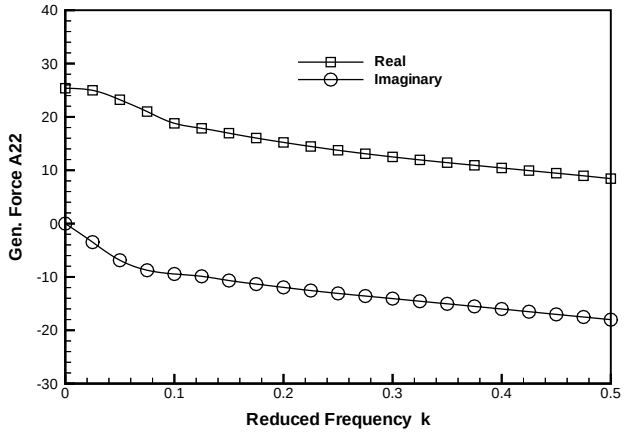

Figure 15: Generalized aerodynamic force Q_{22} for $M_\infty = 0.960$

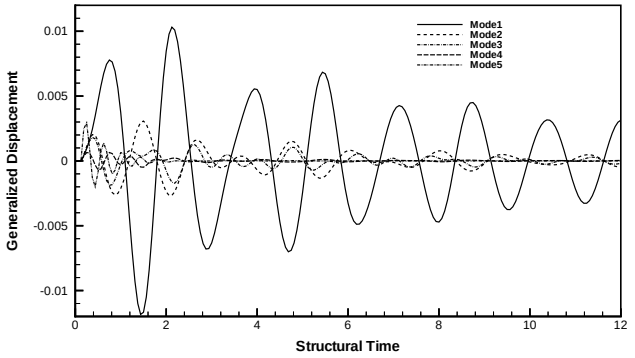

Figure 16: Time history of the generalized coordinates for the AGARD 445.6 wing for $M_\infty = 1.141$ and $V_f = 0.58$.

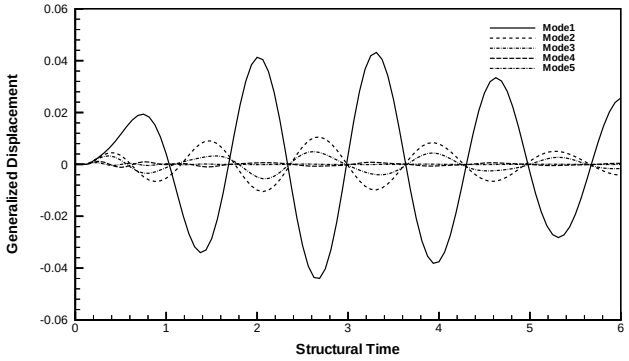

Figure 17: Time history of the generalized coordinates for the AGARD 445.6 wing for $M_\infty = 1.141$ and $V_f = 0.652$.

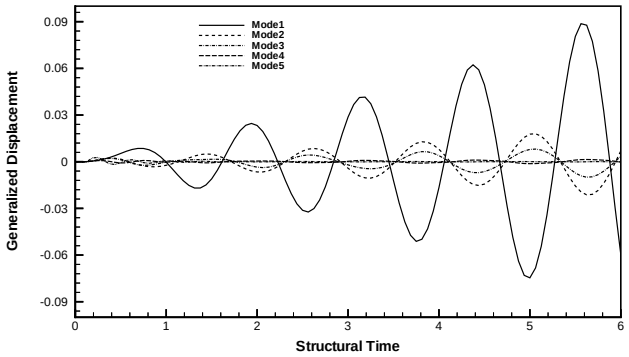

Figure 18: Time history of the generalized coordinates for the AGARD 445.6 wing for $M_\infty = 1.141$ and $V_f = 0.70$.

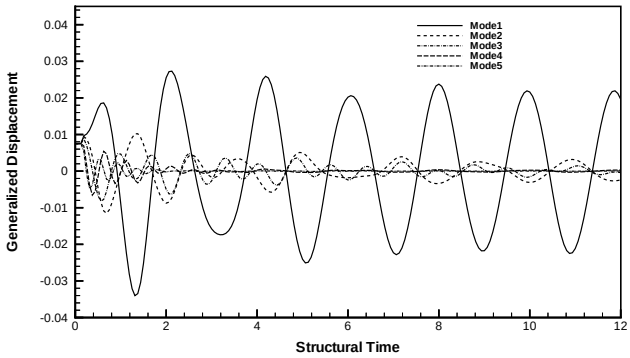

Figure 19: Time history of the generalized coordinates for the AGARD 445.6 wing for $M_\infty = 1.072$ and $V_f = 0.46$.

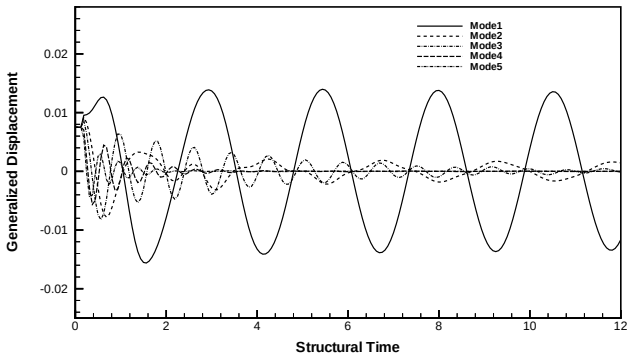

Figure 20: Time history of the generalized coordinates for the AGARD 445.6 wing for $M_\infty = 0.901$ and $V_f = 0.34$.

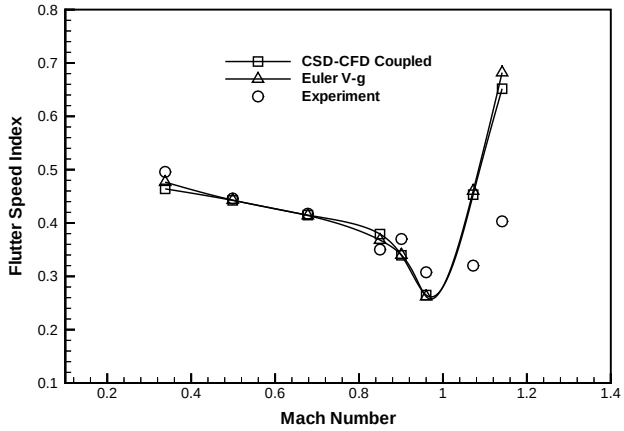

Figure 21: Flutter speed for the AGARD 445.6 Wing.

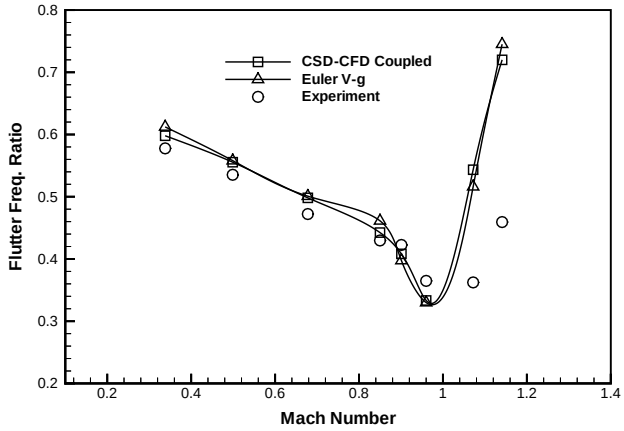

Figure 22: Flutter frequency for the AGARD 445.6 Wing.